Hindawi
Shock and Vibration
Volume 2024, Article ID 7090935, 15 pages
https://doi.org/10.1155/2024/7090935

Research Article

A Bursting Liability Evaluation Method Based on Energy Transfer

Yukun Hou,[1,2] **Shankun Zhao**,[1,2] **and Yang Zhao**[1,2]

[1]*China Coal Research Institute, Beijing 100013, China*
[2]*Mine Safety Technology Branch of China Coal Research Institute, Beijing 100013, China*

Correspondence should be addressed to Shankun Zhao; 641137844@qq.com

Received 8 March 2023; Revised 22 November 2023; Accepted 27 November 2023; Published 8 January 2024

Academic Editor: Antonio Giuffrida

As coal mining gradually moves to deep earth, rock bursts have emerged as one of the main disasters threatening the safety of coal production. It is beneficial to conduct economic and effective prevention and control work by evaluating the bursting liability and improving the bursting liability evaluation system. In this paper, based on the energy transfer model, the relationship between the bursting energy index and the mechanical parameters of coal bodies is obtained by testing the bursting liability of 16 coal seams stratified in three coal mines. According to the bursting energy index and the elastic energy index, the parameter φ is defined to represent the energy release ratio of coal. This paper thus presents a method to evaluate the bursting liability as the product of the energy release ratio and energy transfer ratio and provides a definition for the energy transfer index. The results show that the bursting energy index of coal is closely related to its mechanical parameters. The prepeak deformation energy exhibits a strong positive correlation with uniaxial compressive strength and peak strain. The energy release ratio parameter φ and bursting energy index have high sensitivity and wide applicability. The results of the energy transfer index $\Omega = \beta\varphi$ are consistent with the results of bursting liability identification, which can better reflect the bursting liability, and can be used as the basis for judgment when the "$*$" result is obtained in bursting liability identification. It is anticipated that this approach will become an important evaluation index for bursting liability identification.

1. Introduction

Decreasing shallow coal resources has led the coal mining industry to rapidly turn to deep mining [1]. The frequency of occurrence and degree of danger related to dynamic rock burst disasters in deep coal mines are increasing [2], and such disasters have become one of the major factors threatening safe coal mining activities [3–7]. Understanding the mechanisms associated with rock bursts has led to a large number of theoretical and experimental studies [8–11]. Many theoretical models have been proposed, including stiffness theory, strength theory, energy theory, bursting liability theory, deformation system instability theory, and "three factors" theory [12, 13]. By defining rock bursts [14–21] as a dynamic phenomenon involving coal and rock interactions during mining, studies have addressed the processes by which coal and rock masses gradually transform from static equilibrium to dynamic instability. Under the action of high ground stress, coal-rock masses around the coal mine roadway or working face will be destroyed due to the instantaneous release of elastic energy, which is often accompanied by huge sound, coal-rock mass being thrown into the mining space, and airwaves. These events often cause the destruction of support equipment and the deformation of the mining space; in serious cases, casualties and major damage to the shaft and roadway can occur, as well as surface collapse and local earthquake events.

The main means to evaluate whether a mine is at risk of rock burst events involves the evaluation of the bursting liability grade of a working face or coal seam. This necessitates a bursting liability test on coal samples from within the identification range. Identification work is performed according to national standard GB/T 23561.1-2009, "Methods for determining the physical and mechanical properties of coal and rock Part 1: General requirements for sampling," coal body sampling sample preparation, according to the national standard GB/T 25217.2-2010, and "Methods for test, monitoring, and prevention of rock burst-

Part 2: Classification and laboratory test method on bursting liability of coal (hereinafter referred to as "Standard")." The duration of dynamic fracture, elastic strain energy index, bursting energy index, and uniaxial compressive strength are calculated, and the bursting liability grade is determined according to an evaluation index (Table 1).

The definitions of the bursting energy index and elastic strain energy index are shown in Figure 1; their calculation formulas are as follows:

$$K_E = \frac{U_S}{U_X}, \qquad W_{ET} = \frac{\phi_{SP}}{\phi_{ST}}, \tag{1}$$

where K_E is the bursting energy index, U_S is the deformation energy accumulated before the peak, U_X is the deformation energy consumed after the peak, W_{ET} is the elastic strain energy index, Φ_{SE} is the elastic strain energy, and Φ_{SP} is the plastic strain energy.

The current classification method of bursting liability is based on the statistics of a large number of mine-measured results, which has certain theoretical limitations. It is, therefore, necessary to improve the evaluation theory and method in order to achieve more accurate identifications of bursting liability. On the theoretical basis of Mohr–Coulomb, Zhang et al. [22] put forward a mathematical basis of judgment for coal seam bursting liability, termed the shock buckling stress index. In general, higher stress values are more likely to be greater than the stress index, correlating with higher probabilities of coal seam shock instability. By conducting bursting liability tests of coal, Zuo et al. [23] found that prepeak and postpeak energy dissipation increased with increasing uniaxial compressive strength. When compared with coal sample monomers, the bursting energy index of both coal and rock masses increases, thereby improving impact liability. Deng [24] performed a Hopkinson pressure bar test and numerical simulations for typical coal rocks and determined the dynamic evaluation of coal-rock impact risks by considering the wave velocity anomaly, wave velocity gradient, stress anomaly, and stress gradient indices as evaluative metrics. Gao et al. [25] used MTS815.03 servocontrolled rock mechanics test system to test the coal, rock, and combined specimens with the buried depth of nearly 1200 m in Xinwen Mining Area and analyzed the mechanical properties, energy evolution, and blasting performance. Xu et al. [26] used uniaxial compression tests to determine the mechanical properties and bursting liability of specimens of coal-rock composites with rock partings with different dip angles and thicknesses. Ji et al. [27] combined with Weibull distribution to construct a creep damage constitutive model that can describe the whole process of coal-rock creep and analyzed the impact of impact disturbance on coal-rock creep damage under different initial creep stress and different impact energy.

Based on the energy transfer of coal seams, this paper constructs an energy transfer model for a coal seam, defines the parameters of energy transfer efficiency, and establishes and validates a method by which the bursting liability may be characterized as a product of the energy release and energy transfer ratios through identification tests of bursting liability in several coal seams.

Table 1: Standard for classification of coal bursting tendency.

Parameter	*Bursting liability grade*		
	None	Weak	Strong
Duration of dynamic fracture (ms)	DT > 500	50 < DT ≤ 500	DT ≤ 50
Elastic strain energy index	$W_{ET} < 2$	$2 \le W_{ET} < 5$	$W_{ET} \ge 5$
Bursting energy index	$K_E < 1.5$	$1.5 \le K_E < 5$	$K_E \ge 5$
Uniaxial compressive strength (MPa)	$R_c < 7$	$7 \le R_c < 14$	$R_c \ge 14$

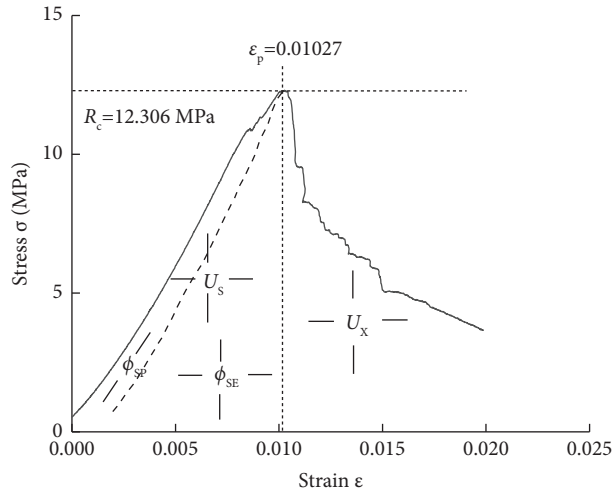

Figure 1: Schematic diagram showing the energy index calculation method.

2. Test Scheme and Results

The main coal seams of three coal mines (M, Y, Z) were selected for sampling tests: the M2 (buried depth 355.17 m), M3-1 (393.69 m), M3-2 (403.02 m), M4-3 (414.66 m), and M6 (475.01 m) coal seams in mine M; the Y1 (368.92 m), Y2 (392.75 m), Y14 (611.45 m), and Y15 (628.86 m) coal seams in mine Y; the Z2 (638.20 m), Z6 (694.02 m), and Z7 (703.62 m) coal seams in mine Z. The coal seam number is arranged from top to bottom according to the burial depth in the area. These seams were identified after sampling according to the requirements of the standard. A GCTS-RTR-4600 test instrument was used. The coal bodies of these three seams are classified as hard coal with high uniaxial compressive strength; some representative samples are shown in Figure 2.

The results of the bursting energy index in the identification test are shown in Table 2, and the stress-strain curves of the impact energy of 81 standard coal specimens were obtained. The stress-strain curves are classified into five types: (1) ordinary, (2) prepeak fluctuation, (3) postpeak

Figure 2: Representative partial coal samples.

fluctuation, (4) postpeak stress precipitous, and (5) postpeak strain rebound. The number of samples without fluctuation or featuring a sudden drop in the whole process accounted for 9.9% of the total samples analyzed. The test results demonstrate that the proportion of "perfect" stress-strain curves obtained when performing the bursting energy index test is less than 10%. The uniaxial compressive strength of coal was found to be relatively large, and the postpeak performance is mainly a "sudden stress drop" in nature.

3. Energy and Mechanical Characteristics of Coal

The bursting energy index represents the ratio of prepeak and postpeak deformation energy of coal. The prepeak curve area includes the dissipated energy and stored elastic deformation energy of coal. The area of the postpeak curve includes mainly the dissipated deformation energy of the coal mass. The main mechanical parameters in the bursting energy index test are uniaxial compressive strength R_c, strain at peak stress, peak strain ε_p, and the elastic modulus E.

The prepeak deformation energy can be expressed by the integral of the stress-strain curve as shown in the following equation:

$$U_S = \int \mathrm{AL}\sigma d\varepsilon \approx \mathrm{AL}\sum_{i=1}^{n} \frac{\sigma_i + \sigma_{i+1}}{2}\left(\varepsilon_{i+1} - \varepsilon_i\right). \quad (2)$$

Equation (3) is then used to correlate the approximate triangular area with the mechanical parameters of coal to form a control:

$$U_S \approx \frac{1}{2}\varepsilon_p \mathrm{ALR}_c, \quad (3)$$

where U_S is the deformation energy accumulated in the prepeak stage of uniaxial compression, σ is the stress, ε is the strain, A is the cross sectional area of the specimen, L is the specimen height, R_c is the uniaxial compressive strength, and ε_p is the peak strain.

The uniaxial compressive strength R_c of the tested coal is 7.87–56.3 MPa, and the peak strain ε_p is 0.41%–2.51%. The total prepeak deformation energy is 4.49–122.43 J, according to (2). According to (3), the prepeak deformation energy is 5.05–138.21 J.

According to the comparison between the two energy calculation methods given in Figure 3, the approximate area of the triangle is slightly larger than the integral result; however, both exhibit a good linear relationship.

Considering the coal deformation energy prior to failure, uniaxial compressive strength, and peak strain, Figure 4(a) shows a strong positive correlation between the three values. As shown in Figures 4(b)–4(d), a power function relationship exists between the deformation energy of coal and its uniaxial compressive strength and an exponential function relationship exists with respect to peak strain. There is a weak power function relationship between peak strain and uniaxial compressive strength. Among the three values, the uniaxial compressive strength of the coal body has the most significant influence on the deformation energy; that is, the deformation energy of the coal body can be roughly inferred from the uniaxial compressive strength to provide a preliminary judgment concerning the bursting energy index and bursting liability.

Figure 5 shows the relationship between the bursting energy index grade of each coal sample tested and its uniaxial compressive strength. Uniaxial compressive strength has a significant influence on the bursting energy index. When the uniaxial compressive strength is greater than 14 MPa, the bursting energy index of the coal body is weak. The uniaxial compressive strength of coal bodies with strong results is almost always greater than 14 MPa. This result is consistent with current standards.

The bursting energy index is also related to postpeak failure processes. Test results show no significant relationships between failure and the postpeak curve of coal mass and uniaxial compressive strength.

4. Energy Release Ratio

Uniaxial compressive strength is a mechanical parameter with greater weight in the existing bursting liability evaluation system. Consequently, an energy release ratio was introduced to construct an evaluation index of bursting liability from the perspective of energy transfer.

4.1. Definition of the Energy Release Ratio φ. The energy release ratio is defined as the ratio between the impact energy released during coal failure and the elastic deformation energy obtained during coal loading, thereby reducing the ratio of energy released by coal destruction to energy. The impact energy released during the coal failure process under compression is equal to the difference between the elastic deformation energy obtained before failure and the dissipated deformation energy after failure. The elastic deformation energy is equal to the integrated area of the prepeak stress-strain curve minus dissipated energy in the calculation of the elastic energy index.

According to Figure 1, the elastic energy index and bursting energy index can be used to calculate and characterize the energy release ratio φ as follows:

$$\varphi = \frac{\phi_{\mathrm{SE}} - U_X}{\phi_{\mathrm{SE}}} = 1 - \frac{W_{\mathrm{ET}} + 1}{W_{\mathrm{ET}} K_E}. \quad (4)$$

Figure 6 shows the relationship between the positive φ range of energy release ratio after coal mass failure and the two energy indexes, both of which show a positive

Table 2: Results of bursting energy index test.

Specimen	Bursting energy index K_E	Uniaxial compressive strength R_C (MPa)	Peak strain (%)	Stress-strain curve characteristics	Prepeak curve features	Postpeak curve features	Prepeak deformation energy U_S (J)	Postpeak deformation dissipated energy U_X (J)
M2-1	9.929	15.340	1.018	2	Multiple stress drop	—	16.403	1.652
M2-2	9.971	56.300	2.505	4	—	One data point	122.432	12.280
M2-3	24.974	24.170	1.626	4	—	Few data point	32.712	1.310
M2-4	5.577	18.330	1.636	2&3	Multiple stress drop	Failures after softening	28.971	5.195
M2-5	34.704	21.650	1.034	2&3	Once stress drop	Softening	21.233	0.612
M3-1-1	4.714	13.092	0.653	5	—	Fluctuating	8.361	1.773
M3-1-2	3.757	11.737	1.047	2	Fluctuating	—	14.681	3.907
M3-1-3	2.204	18.530	1.255	3	—	Multiple rebound	21.239	9.637
M3-1-4	2.205	16.600	0.819	2	Multiple stress drop	—	14.294	6.483
M3-1-5	3.060	20.300	1.014	2&3	Multiple stress drop	Multiple rebound	22.225	7.263
M3-2-1	3.245	23.610	1.027	4	—	Softening	23.073	7.110
M3-2-2	1.399	10.866	0.986	2&3	Fluctuating	Fluctuating	14.249	10.183
M3-2-3	3.935	23.783	1.107	3	—	Fluctuating	25.158	6.393
M3-2-4	4.627	27.557	1.697	3	—	Fluctuating	41.491	8.967
M3-2-5	6.846	26.856	1.186	1	—	—	29.582	4.322
M4-3-1	2.082	8.353	0.481	3	—	Fluctuating	4.276	2.054
M4-3-2	2.286	11.302	0.729	3	—	Softening	8.447	3.695
M4-3-3	2.559	16.254	0.798	3	—	Fluctuating	12.437	4.862
M4-3-4	3.197	26.275	0.716	3	—	Fluctuating	18.522	5.794
M4-3-5	1.119	12.306	1.027	1	—	—	12.749	11.388
M6-1	6.044	19.530	0.952	1	—	—	16.963	2.806
M6-2	8.213	18.970	0.922	1	—	—	17.683	2.154
M6-3	—	16.720	0.523	5	—	Strain rebound	7.897	0.010
M6-4	42.119	22.370	1.035	4	—	Sudden drop	20.167	0.479
M6-5	95.270	20.550	0.940	4	—	Sudden drop	19.060	0.200
Y1-1	5.127	16.030	1.111	2&3&4	Fluctuating	Sudden drop, fluctuating, and sudden drop	21.153	4.125
Y1-2	1.008	7.870	0.554	1	—	—	5.474	5.433
Y1-3	2.690	17.040	0.852	4	—	Sudden drop	14.846	5.521
Y1-4	3.708	19.910	1.029	4	—	Sudden drop	20.554	5.543
Y1-5	2.472	15.860	0.819	4	—	Sudden drop	11.973	4.848
$Y2_1$-1	4.786	13.630	0.693	2&3&4	Rebounds once	Sudden drop, rebounding once, and sudden drop	11.135	2.327
$Y2_1$-2	2.656	27.200	1.326	4	—	Sudden drop, softening, and sudden drop	34.212	12.882
$Y2_1$-3	1.923	13.990	0.671	3&4	—	Rebound once and sudden drop	9.876	5.135

Table 2: Continued.

Specimen	Bursting energy index K_E	Uniaxial compressive strength R_C (MPa)	Peak strain (%)	Stress-strain curve characteristics	Prepeak curve features	Postpeak curve features	Prepeak deformation energy U_S (J)	Postpeak deformation dissipated energy U_X (J)
$Y2_1$-4	118.230	37.680	1.863	4	—	Sudden drop	64.363	0.544
$Y2_1$-5	13.432	18.820	1.038	2&3&4	Rebounding once	Sudden drop, rebounding once, and sudden drop	21.616	1.610
$Y2_2$-1	2.150	17.180	0.833	2&3&4	Rebounding once	Sudden drop and sudden drop	14.051	6.536
$Y2_2$-2	8.194	15.090	0.932	4	—	Sudden drop	16.085	1.962
$Y2_2$-3	3.829	15.980	0.853	4	—	Sudden drop	14.506	3.788
$Y2_2$-4	4.363	16.420	1.020	3&4	—	Sudden drop	18.744	4.267
$Y2_2$-5	2.132	16.990	0.939	2&3	Fluctuating	Fluctuating	18.396	8.626
$Y2_3$-1	9.435	34.680	1.838	4	—	Sudden drop	60.811	6.446
$Y2_3$-2	51.796	38.100	1.869	4	—	Sudden drop	69.135	1.335
$Y2_3$-3	1.785	13.480	0.997	1	—	—	14.930	8.363
$Y2_3$-4	15.477	18.690	0.982	4	—	Sudden drop	19.156	1.237
$Y2_3$-5	4.546	15.030	0.862	4	—	Sudden drop	12.551	2.761
Y14-1	6.325	25.880	1.088	4	—	Sudden drop	28.319	4.477
Y14-2	3.648	16.060	0.736	4	—	Sudden drop	13.843	3.793
Y14-3	2.996	20.810	0.997	4	—	Sudden drop	20.246	6.758
Y14-4	1.941	19.300	0.750	4	—	Sudden drop	14.789	7.618
Y14-5	40.829	35.180	1.719	4	—	Sudden drop	60.340	1.479
Y14-6	1.438	14.230	0.743	2&3	Fluctuating	Strain rebound	11.210	7.795
Y15-1	7.131	19.660	0.955	4	—	Sudden drop	18.262	2.560
Y15-2	1.730	13.620	0.686	3	—	Multiple rebound	9.839	5.688
Y15-3	6.617	13.100	1.036	4	—	Sudden drop	15.184	2.295
Y15-4	2.379	13.050	0.721	4	—	Sudden drop	10.139	4.263
Y15-5	1.509	13.960	0.860	1	—	—	12.362	8.192
$Z2_1$-1	4.946	16.010	0.896	1	—	—	13.631	2.757
$Z2_1$-2	3.880	13.740	0.717	3	—	Fluctuating	10.291	2.653
$Z2_1$-3	7.797	21.090	0.792	4	—	Sudden drop	17.436	2.236
$Z2_1$-4	4.437	21.050	0.745	4	—	Sudden drop	15.274	3.442
$Z2_1$-5	5.630	19.850	0.730	2&4	Fluctuating	Sudden drop	15.086	2.680
$Z2_2$-1	2.042	12.940	0.659	4	—	Sudden drop	9.468	4.636
$Z2_2$-2	0.764	10.080	0.413	3	—	Fluctuating	4.494	5.887
$Z2_2$-3	1.330	10.770	0.439	3	—	Fluctuating	5.150	3.874
$Z2_2$-4	8.202	20.670	0.900	4	—	Sudden drop	18.162	2.215
$Z2_2$-5	8.038	16.950	0.899	4	—	Sudden drop	16.432	2.044
$Z2_3$-1	1.734	10.880	0.518	2&3	Fluctuating	Fluctuating	6.344	3.660
$Z2_3$-2	7.385	19.090	0.924	4	—	Sudden drop	19.291	2.611
$Z2_3$-3	2.412	14.030	0.652	4	—	Sudden drop	10.403	4.314
$Z2_3$-4	1.941	12.710	0.776	2&3	Fluctuating	Fluctuating	11.667	6.012
$Z2_3$-5	2.390	18.730	0.857	2&4	Sudden drop	Fluctuating and sudden drop	16.067	6.723
Z6-1	4.687	15.170	0.755	4	—	Sudden drop	12.172	2.598

Table 2: Continued.

Specimen	Bursting energy index K_E	Uniaxial compressive strength R_C (MPa)	Peak strain (%)	Stress-strain curve characteristics	Prepeak curve features	Postpeak curve features	Prepeak deformation energy U_S (J)	Postpeak deformation dissipated energy U_X (J)
Z6-2	2.992	16.380	0.753	4	—	Sudden drop	13.171	4.402
Z6-3	0.885	13.800	0.591	2	Fluctuating	—	8.873	10.026
Z6-4	1.383	13.660	0.660	3	—	Fluctuating	9.749	7.051
Z6-5	—	20.920	0.898	5	—	Strain rebound	19.651	0.000
Z7-1	1.983	8.770	0.994	2&3	Fluctuating	Fluctuating	11.215	5.655
Z7-2	4.584	15.860	0.801	4	—	Sudden drop	12.784	2.788
Z7-3	2.720	15.620	0.779	2&3	Fluctuating	Fluctuating	14.669	5.394
Z7-4	2.373	27.910	1.504	4	—	Sudden drop	39.796	16.770
Z7-5	1.923	12.030	0.492	4	—	Sudden drop	5.604	2.914

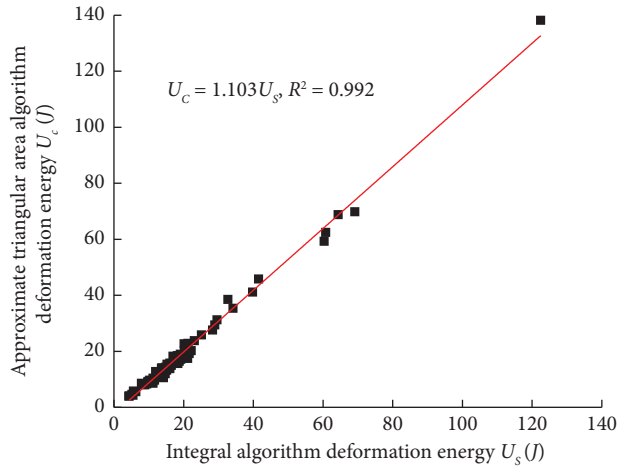

Figure 3: Scatter diagram showing the relationship between the estimated deformation energy and observed values.

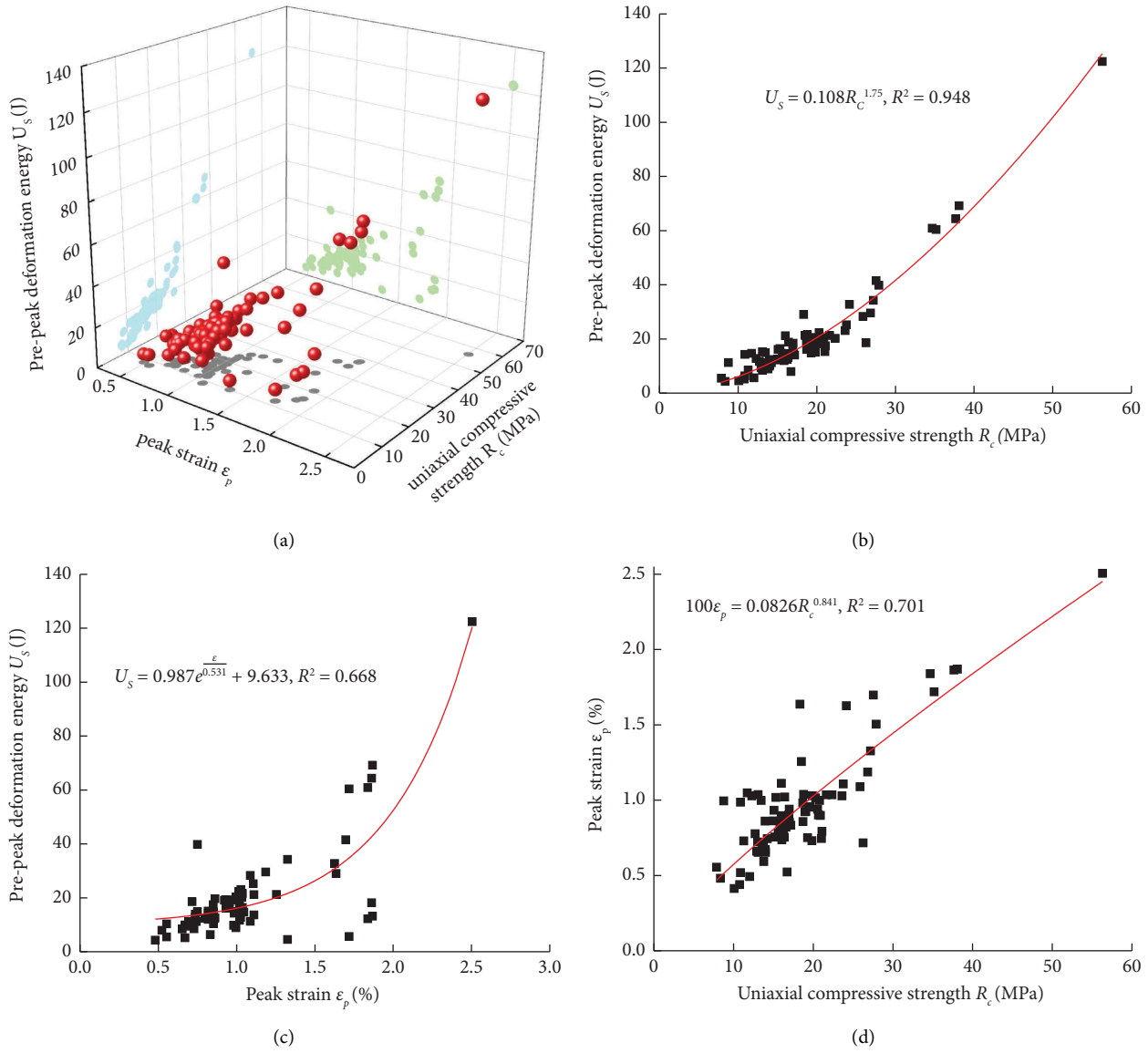

Figure 4: (a) Scatter diagram showing the relationship between deformation energy and uniaxial strength and peak strain. (b) Scatter diagram showing the relationship between deformation energy and uniaxial compressive strength. (c) Scatter diagram showing the relationship between deformation energy and peak strain. (d) Scatter diagram showing the relationship between peak strain and uniaxial compressive strength.

correlation; the bursting energy index is shown to have a higher sensitivity.

The energy transfer process in coal seams is regarded as a chain reaction of energy to the roadway or working face such that the ability of coal bodies in each area of the coal seam to transfer energy to adjacent areas determines the impact risk. A necessary condition for the occurrence of rock bursts is continuous energy transfer within the coal seam. According to the definition of the energy release ratio, when the energy release ratio $\varphi < 0$, the coal body does not release impact energy to the outside; thus, coal bodies meeting this condition tend to not continuously transfer energy. Under such conditions, the coal seam is not liable to burst. Conversely, when $\varphi > 0$, in addition to being dissipated by deformation energy, a certain proportion of energy is released to adjacent coal bodies; such coal bodies may have bursting liability. When $\varphi = 0$, the system is at the critical point of rock burst, and equation (5) can be obtained from equation (4) as follows:

$$K_E = 1 + \frac{1}{W_{\mathrm{ET}}}. \tag{5}$$

Several groups of critical values related to the bursting liability index are $(K_E, W_{\mathrm{ET}}) = \{(1.2, 5), (1.5, 2), (5, 0.25)\}$. These are consistent with the critical value of the bursting liability identification index, indicating that it is reasonable and feasible to use the energy release proportion parameter φ to classify the bursting liability grade due to energy transfer.

4.2. Analysis of Experimental Results of Energy Release Ratio φ. Because the bursting energy index and elastic energy index cannot be obtained from the same specimen and because the bursting energy index is highly sensitive, the bursting energy index is taken as the test value and then the elastic energy index is taken as the average value of the stratified test results. According to the elastic energy index test of each coal seam in the three mines examined, the average elastic energy indices of each coal seam layer can be obtained as follows: M2 (22.546); M3-1 (13.538); M3-2 (13.003); M4-3 (10.339); M6 (19.743); Z2 (21.216); Z6 (21.961); Z7 (21.147); Y1 (18.772); Y2 (23.747); Y14 (14.180); and Y15 (31.954).

After obtaining the calculated results (Table 3 and Figure 7(a)), the bursting liability of 19 coal layers according to the author's unit was determined (Figure 7(b)). Finally, all results were integrated to obtain Figure 7(c). The distribution of the bursting energy index and energy proportion φ under three data conditions at the mean elastic energy index value is shown in Figures 7(a)–7(c). These results show that the energy release ratio can achieve fitting convergence for different coal seams in different coal mines and has wide applicability. Based on the energy release ratio parameter, this paper reuses the bursting energy index and elastic energy index and combines the energy transfer efficiency to construct an evaluation index of bursting liability, termed the energy transfer index.

5. Evaluation Index of Bursting Liability (Energy Transfer Index)

5.1. Energy Transfer Model. Qi et al. [28] proposed the concepts of "stress flow" and "energy flow," showing that energy transfer in coal has the property of the field. Three hypotheses can be made as follows. Hypothesis 1: when a coal body releases energy, most energy propagates in the opposite direction of energy storage, and the propagation ratio of multiple directions is positively correlated with the form of energy storage. Hypothesis 2: energy transfer occurs along a continuous path. Hypothesis 3: energy transfer velocity is consistent with stress transfer velocity. On this basis, a model for transferring large-scale energy to the roadway through the coal seam may be built, as shown in Figure 8.

The coal seam was then divided into several blocks. When large energy sources are transferred to the coal seam at a distance, the energy transferred by coal bodies in each region can be simplified into three conditions: (1) regional large-scale destructive transfer; (2) coexisting failure and elastic propagation; and (3) only elastic propagation. For regional large-scale failure transfer, the energy is far greater than the instability limit of the coal mass. Consequently, a rock burst with large-scale failure will occur, and it is meaningless to study the energy transfer efficiency between coal masses. In the case of elastic propagation only, the energy is stored in the coal body in the form of elastic energy during the transfer process and shows a state of gradual dissipation, finally showing an increase in the overall energy storage of the coal seam; this will not result in a rock burst. When elasticity and destructive transfer coexist, coal initially absorbs the impact energy into its own elastic energy and then transfers the elastic energy to the next region. After reaching its limit, the coal becomes unstable and fails, releasing the impact energy into the next region. Finally, a chain reaction of continuous instability of coal in each region is formed.

5.2. Energy Transfer Efficiency. As shown in Figure 8, when energy is transferred to the coal seam, it begins at region X_1 and ends at the roadway. The size and form of the energy finally transferred to the roadway determine whether the energy source will trigger a rock burst. Based on energy flow assumptions, most energy will be transferred along a path such that the proportion of the energy released by the upstream coal body to the downstream coal body per unit volume in the energy flow field is defined as the energy transfer proportion β. The energy initially accumulated by coal X_n in each region of the coal seam is taken to be U_n, and the energy released to the downstream path after instability failure is a_{n}. Beginning with the release of energy U_0 in the upstream path, which is transferred to the coal mass in region X_1, the interregional energy transfer value a_i can be obtained using the energy release ratio φ and energy transfer ratio β, as shown in the following equation:

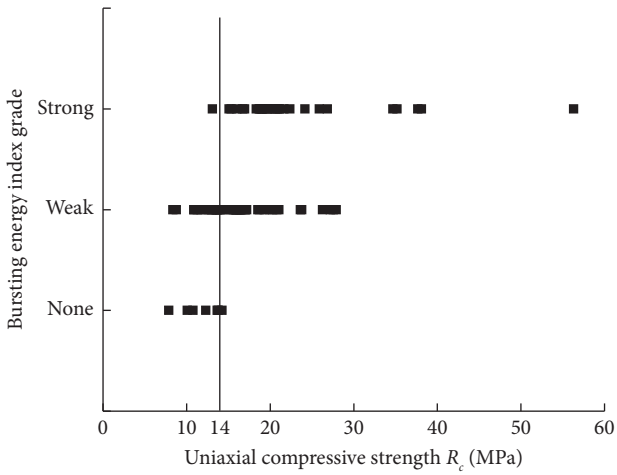

Figure 5: Scatter diagram showing bursting energy index grade and uniaxial compressive strength.

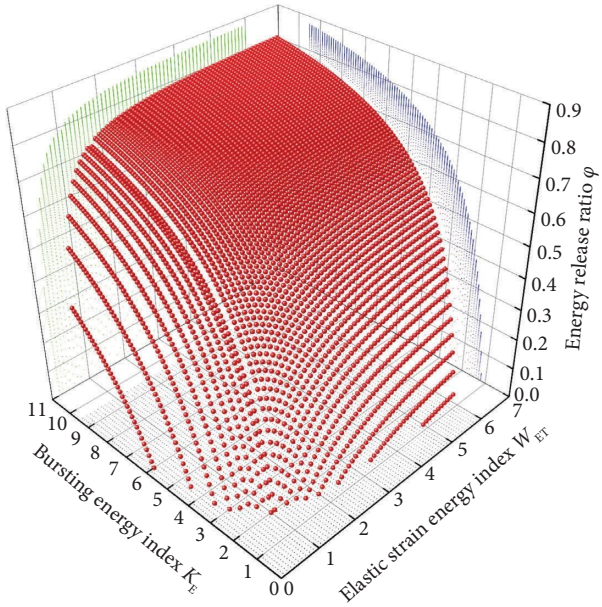

Figure 6: Theoretical relationship between the energy release ratio and bursting energy index and elastic energy index.

$$
\begin{aligned}
a_0 &= U_0\beta\varphi,\\
a_1 &= (U_1 + a_0)\beta\varphi = U_1\beta\varphi + U_0(\beta\varphi)^2,\\
a_2 &= (U_2 + a_1)\beta\varphi = U_2\beta\varphi + U_1(\beta\varphi)^2 + U_0(\beta\varphi)^3,\\
a_3 &= (U_3 + a_2)\beta\varphi = U_3\beta\varphi + U_2(\beta\varphi)^2 + U_1(\beta\varphi)^3 + U_0(\beta\varphi)^4,\\
&\cdots\\
a_n &= U_n\beta\varphi + U_{n-1}(\beta\varphi)^2 + \cdots + U_0(\beta\varphi)^{n+1} = \sum_{i=0}^{n} U_n(\beta\varphi)^{i+1}.
\end{aligned}
\tag{6}
$$

Assuming that the initial energy storage discretization of coal masses in each area of the coal seam is low, $U_{1\sim n}$ is uniformly simplified to U. In general, U_0 is greater than U, and the negative energy release ratio is not considered. Let $0 \le \varphi \le 1$. Equation (6) can be simplified as follows:

$$
\begin{aligned}
a_n &= U\frac{\beta\varphi - (\beta\varphi)^{n+1}}{1-\beta\varphi} + U_0(\beta\varphi)^{n+1},\\
a_{n\longrightarrow\infty} &= U\frac{\beta\varphi}{1-\beta\varphi}.
\end{aligned}
\tag{7}
$$

Table 3: Calculation results of the energy release ratio.

Specimen	φ
M2-1	0.895
M2-2	0.895
M2-3	0.958
M2-4	0.813
M2-5	0.970
M3-1-1	0.772
M3-1-2	0.714
M3-1-3	0.513
M3-1-4	0.513
M3-1-5	0.649
M3-2-1	0.668
M3-2-2	0.230
M3-2-3	0.726
M3-2-4	0.767
M3-2-5	0.843
M4-3-1	0.473
M4-3-2	0.520
M4-3-3	0.571
M4-3-4	0.657
M4-3-5	0.020
M6-1	0.826
M6-2	0.872
M6-3	—
M6-4	0.975
M6-5	0.989
$Z2_1$-1	0.788
$Z2_1$-2	0.730
$Z2_1$-3	0.866
$Z2_1$-4	0.764
$Z2_1$-5	0.814
$Z2_2$-1	0.487
$Z2_2$-2	−0.371
$Z2_2$-3	0.213
$Z2_2$-4	0.872
$Z2_2$-5	0.870
$Z2_3$-1	0.396
$Z2_3$-2	0.858
$Z2_3$-3	0.566
$Z2_3$-4	0.461
$Z2_3$-5	0.562
Y1-1	0.795
Y1-2	−0.045
Y1-3	0.608
Y1-4	0.716
Y1-5	0.574
$Y2_1$-1	0.782
$Y2_1$-2	0.608
$Y2_1$-3	0.458
$Y2_1$-4	0.991
$Y2_1$-5	0.922
$Y2_2$-1	0.515
$Y2_2$-2	0.873
$Y2_2$-3	0.728
$Y2_2$-4	0.761
$Y2_2$-5	0.511
$Y2_3$-1	0.890
$Y2_3$-2	0.980
$Y2_3$-3	0.416
$Y2_3$-4	0.933
$Y2_3$-5	0.771
Y14-1	0.831
Y14-2	0.707
Y14-3	0.643
Y14-4	0.448
Y14-5	0.974
Y14-6	0.256
Y15-1	0.855
Y15-2	0.404
Y15-3	0.844
Y15-4	0.567
Y15-5	0.317
Z6-1	0.777
Z6-2	0.651
Z6-3	−0.181
Z6-4	0.244
Z6-5	—
Z7-1	0.472
Z7-2	0.772
Z7-3	0.615
Z7-4	0.559
Z7-5	0.455

It is then facile to demonstrate that when $\beta\varphi = 0.5$, the transfer efficiency at infinity $a_n/U = 1$, and when $0 < \beta\varphi < 0.5$, the energy transfer efficiency at infinity is always less than 1. When $\beta\varphi > 0.5$, the transfer efficiency is greater than 1 at noninfinite distances; that is, the total amount of energy involved in the energy transfer process is gradually enlarged. For coal seams that are not in a critical state of instability, it is difficult to form a chain reaction when the transfer efficiency is less than 1. Conversely, when the transfer efficiency is greater than 1, a chain reaction of continuous failure may occur, thus triggering rock bursts at the end point of the roadway, which functions as the transfer path.

5.3. Calculation of the Energy Transfer Ratio β. According to the energy flow hypothesis, the direction of energy release is inversely related to the time of energy storage, whereas the magnitude is positively correlated. The energy release ratio φ represents the energy dissipation ratio, and the energy transfer ratio β represents the energy propagation ratio along the path. The direction of the transfer path is defined as the main direction, the energy transferred to the main direction is U_m, and the energy dissipated vertically and horizontally orthogonal to the main direction are U_{v1} and U_{v2}, respectively. Then, the energy transfer ratio parameter β in the main direction during the failure of regional coal mass can be expressed as follows:

$$\beta = \frac{U_m}{U_m + U_{v1} + U_{v2}}. \tag{8}$$

The product of the three parameters of section $A(t)$ length $L(t)$ stress $\sigma(t)$ in the affected region is expressed as the following function:

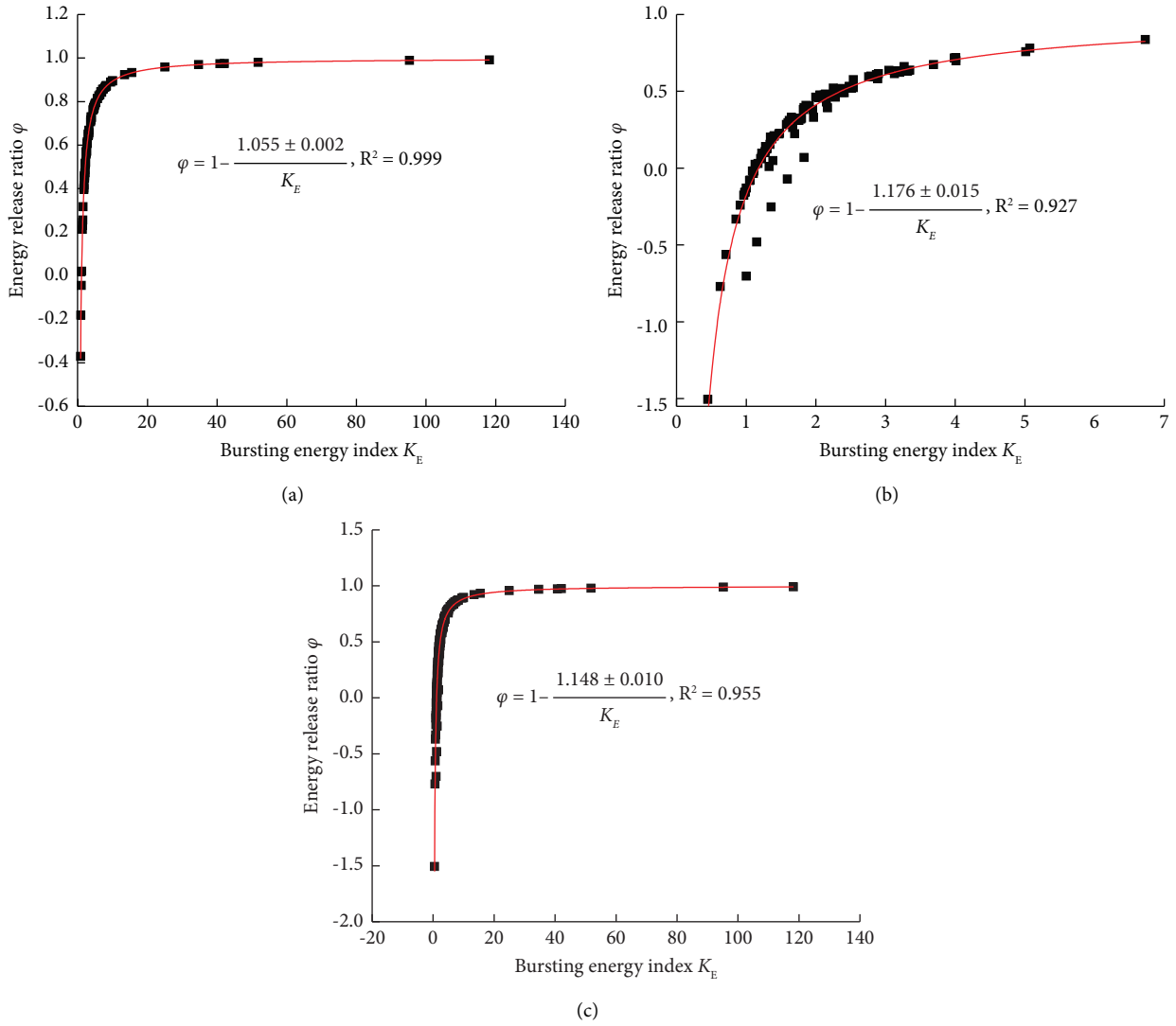

Figure 7: Relationships between energy release ratio and bursting energy index. (a) Test results of M, Y, and Z mines. (b) Extraction results of 19 coal seam identification reported. (c) Comprehensive results.

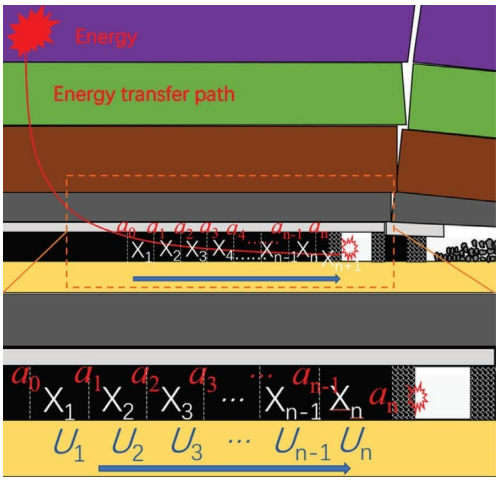

Figure 8: Energy transfer process model in a coal seam.

$$g(t) = A(t)L(t)\sigma(t). \tag{9}$$

The energy transferred by coal in the main direction when energy transfer arrives may be determined using the following formula:

$$U_m = \int g_m(t)\mathrm{d}\varepsilon_m. \tag{10}$$

For U_m and U_v, the strain has a relationship of $\nu_{\varepsilon m} = \varepsilon\nu$, and ν is Poisson's ratio. The energy in the direction orthogonal to the principal direction is as follows:

$$\begin{aligned} U_v &= \int g_{v1}(t)\mathrm{d}\varepsilon_v + \int g_{v2}(t)\mathrm{d}\varepsilon_v \\ &= \int \left(g_{v1}(t) + g_{v2}(t)\right)\nu\mathrm{d}\varepsilon_m. \end{aligned} \tag{11}$$

Substituting into (8), we obtain the following expression:

$$\begin{aligned} \beta &= \frac{U_m}{U_m + U_{v1} + U_{v2}} = \frac{\int g_m(t)\mathrm{d}\varepsilon_m}{\int g_m(t)\mathrm{d}\varepsilon_m + \int g_{v1}(t)\nu\mathrm{d}\varepsilon_m + \int g_{v2}(t)\nu\mathrm{d}\varepsilon_m} \\ &= \frac{\int A_m(t)L_m(t)\sigma_m(t)\mathrm{d}\varepsilon}{\int \left(A_m(t)L_m(t)\sigma_m(t) + \nu A_{v1}(t)L_{v1}(t)\sigma_{v1}(t) + \nu A_{v2}(t)L_{v2}(t)\sigma_{v2}(t)\right)\mathrm{d}\varepsilon}. \end{aligned} \tag{12}$$

As shown in Figure 9, the stress state of the coal unit before and after energy transfer may be constructed. In its initial state, the stress in three directions is small and increases according to the relative fixed proportional coefficient after energy transfer. The main directional stress coefficient k_{m} is defined, with two orthogonal direction stress coefficients of k_1 and k_2, respectively. Further simplifying the boundary conditions obtains the following expression:

$$\frac{\sigma_m(t)}{\sigma_{v1}(t) + \sigma_{v2}(t)} = \frac{k_{\mathrm{m}}}{k_2 + k_1}, \tag{13}$$

$$\begin{aligned} A_m(t) &= A_{v1}(t) = A_{v2}(t), \\ L_m(t) &= L_{v1}(t) = L_{v2}(t). \end{aligned} \tag{14}$$

Assuming that the stress ratio remains almost constant during the energy transfer process, the value of β is obtained by substitution of (13) and (14) into (12) as follows:

$$\begin{aligned} \beta &= \frac{\int \sigma_m(t)\mathrm{d}\varepsilon_m}{\int \left(\sigma_m(t) + \nu\sigma_{v1}(t) + \nu\sigma_{v2}(t)\right)\mathrm{d}\varepsilon_m} \\ &\approx \frac{\sigma_m(t)}{\sigma_m(t) + \nu\sigma_{v1}(t) + \nu\sigma_{v2}(t)} \\ &= \frac{k_m}{k_m + \nu(k_1 + k_2)}. \end{aligned} \tag{15}$$

Equation (15) indicates that the energy transfer proportion is affected by the stress coefficient in the main direction of coal, but it is very difficult to obtain an accurate stress coefficient. Consequently, this paper adopts the boundary condition of the value for analysis. For the uniaxial case, $k_1 = k_2 = 0$ and $\beta = 1$. For the triaxial case, $k_m/k_1 \le 6$ can be obtained from the statistical rule of triaxial compression test data for the three mines examined. For a deep hydrostatic pressure environment, $k_m \ge k_1 = k_2$. For a shallow environment, Xie et al. [29, 30] showed that the horizontal principal stress (tectonic stress) of the coal body was greater than the vertical principal stress in the range of burial depth from 1000 to 400 m, and the ratio range was $k_2/k_1 = 1\sim2$. The value range of the energy transfer ratio is then obtained as follows:

$$\begin{aligned} \frac{1}{1 + 2\nu} \le \beta \le \frac{1}{1 + 1/3\nu}, &\text{ Deep,} \\ \frac{1}{1 + 1.5\nu} \le \beta \le \frac{1}{1 + 0.5\nu}, &\text{ Fallow.} \end{aligned} \tag{16}$$

In order to confirm the accuracy of the evaluation index, the minimum value of the corresponding energy transfer ratio of coal seams with different burial depths was considered. Given that the buried depth of the coal seam in this paper is less than 800 m, it belongs to the shallow range, and the following equation applies:

$$\beta = \frac{1}{1 + 1.5\nu}. \tag{17}$$

5.4. Evaluation Index of Bursting Liability and Energy Transfer Index. Based on the product parameter $\Omega = \beta\varphi$ of energy release ratio and transfer efficiency and taking 0 and 0.5 as critical standards, the bursting liability energy flow index is set as shown in Table 4.

The burst liability evaluation results of mines M, Y, and Z were determined based on the energy release ratio and calculated according to stratified average values, as shown in Table 5.

Identification results labeled " $*$ " in Table 5 indicate that the four indicators measured according to the current standard had uncertain results and needed to be further judged according to their identification values. The results of the energy transfer index are consistent with the total identification results. Therefore, the energy transfer index can be used as the basis of judgment when the

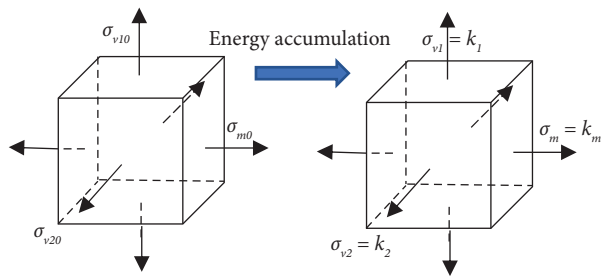

Figure 9: Stress variation of coal during the energy transfer process.

Table 4: Energy release ratio impulse liability index.

Indication range	Formula	Result
$\Omega \le 0$	$W_{ET}K - W_{ET} - 1/(1+\nu)W_{ET}K_E \le 0$	None
$0 < \Omega < 0.5$	$0 < W_{ET}K - W_{ET} - 1/(1+\nu)W_{ET}K_E < 0.5$	Weak
$\Omega \ge 0.5$	$W_{ET}K - W_{ET} - 1/(1+\nu)W_{ET}K_E \ge 0.5$	Strong

Table 5: Validation results of the energy transfer index.

Coal seam	K_E	W_{ET}	Poisson's ratio	Ω result	Standard result
M2	32.569	22.546	0.331	0.647 strong	Strong
M3-1	1.731	13.538	0.342	0.251 weak	*
M3-2	3.224	13.003	0.318	0.451 weak	*
M4-3	1.590	10.339	0.296	0.215 weak	*
M6	9.137	19.743	0.283	0.621 strong	Strong
$Z2_1$	4.535	18.433	0.351	0.503 strong	*
$Z2_2$	3.807	20.568	0.312	0.494 weak	*
$Z2_3$	3.065	24.648	0.292	0.459 weak	*
Z6	2.404	21.961	0.304	0.388 weak	*
Z7	2.575	21.147	0.310	0.405 weak	Weak
Y1	2.853	18.772	0.306	0.432 weak	Weak
$Y2_1$	26.669	20.341	0.294	0.667 strong	Strong
$Y2_2$	3.931	28.909	0.316	0.500 strong	*
$Y2_3$	15.325	21.991	0.263	0.668 strong	Strong
Y14	2.999	14.180	0.286	0.450 weak	*
Y15	3.295	31.954	0.345	0.453 weak	*

comprehensive result of bursting liability is "*" Furthermore, this suggests that the metric can be used as an important reference for bursting liability identification.

6. Conclusion

In this study, bursting liability identification tests have been conducted for 16 layers in three coal mines to determine the bursting liability of coal bodies. Furthermore, the energy release ratio and energy transfer index were defined. The following conclusions were obtained from this study:

(1) The bursting energy index of coal is closely related to its mechanical parameters. A strong positive correlation exists between the prepeak deformation energy, uniaxial compressive strength, and peak strain. When the value of a certain mechanical parameter increases, the values of other parameters will increase; consequently, the prepeak deformation energy and energy accumulation capacity will also increase. No strong correlation was found between the elastic modulus and other mechanical parameters; this is therefore considered a relatively independent mechanical parameter.

(2) The energy release proportion parameter φ is consistent with the values of the elastic energy and bursting energy indices. When compared with the elastic energy index, the energy release ratio φ and bursting energy index have higher sensitivities.

(3) The energy transfer index $\Omega = \beta\varphi = W_{ET}K_E - W_{ET} - 1/(1+1.5\nu)W_{ET}K_E$ can better reflect the bursting liability of coal and can be used as the basis of judgment when the result "*" appears in the

identification of bursting liability. Furthermore, the energy transfer index can be used as an important reference for identifying bursting liability.

Data Availability

The data used to support the findings of this study are available from the corresponding author upon request.

Conflicts of Interest

The authors declare that they have no conflicts of interest.

Authors' Contributions

All authors have read and agreed to the published version of the manuscript.

Acknowledgments

The author acknowledge the financial support provided by the National Science Foundation of China (Grant no. 52034009), Open Fund Project for the Cultivation Base of State Key Laboratory jointly built by the Ministry and the Ministry of Mine Stratum Intelligent Control and Green Mining (Grant no. SICGM202106), and Science and Technology Development Fund Project of China Coal Research Institute (Grant no. 2021CX-II-12).

References

[1] S. C. Li, H. P. Wang, Q. H. Qian et al., "In-situ monitoring research on zonal disintegration of surrounding rock mass in deep mine roadways," *Chinese Journal of Rock Mechanics and Engineering*, vol. 27, no. 8, pp. 1545–1553, 2008.

[2] X. Xu, H. Feng, L. Jiang, T. Guo, X. Wu, and Z. Sun, "Research on deformation and failure evolution of deep rock burst drivage roadway surrounding rock under dynamic disturbance," *Shock and Vibration*, vol. 2021, Article ID 7956421, 13 pages, 2021.

[3] N. Zhou, H. Liu, J. Zhang, and H. Yan, "Study on rock burst event disaster and prevention mechanisms of hard roof," *Advances in Civil Engineering*, vol. 2019, Article ID 6910139, 14 pages, 2019.

[4] Y. D. Jiang, Y. X. Zhao, H. W. Wang, and J. Zhu, "A review of mechanism and prevention technologies of coal bumps in China," *Journal of Rock Mechanics and Geotechnical Engineering*, vol. 9, no. 1, pp. 180–194, 2017.

[5] L. M. Dou, Z. L. Mu, A. Y. Cao, Z. L. Li, and S. Gong, "Research progress of monitoring, forecasting, and prevention of rockburst in underground coal mining in China," *International Journal of Coal Science and Technology*, vol. 1, no. 3, pp. 278–288, 2014.

[6] M. Wu, Y. C. Ye, Q. H. Wang, and N. Y. Hu, "Development of rockburst research: a comprehensive review," *Applied Sciences*, vol. 12, no. 3, p. 974, 2022.

[7] P. Konicek, K. Soucek, L. Stas, and R. Singh, "Long-hole destress blasting for rockburst control during deep underground coal mining," *International Journal of Rock Mechanics and Mining Sciences*, vol. 61, pp. 141–153, 2013.

[8] W. Z. Liang, B. Dai, G. Zhao, and H. Wu, "A scientometric review on rockburst in hard rock: two decades of review from 2000 to 2019," *Geofluids*, vol. 2020, Article ID 8763283, 17 pages, 2020.

[9] H. P. Kang, G. Xu, B. M. Wang et al., "Forty years development and prospects of underground coal mining and strata control technologies in China," *Journal of Mining and Strata Control Engineering*, vol. 1, no. 1, p. 33, 2019.

[10] L. Xu and F. Q. Gong, "Experimental study of strain rockburst considering temperature effect: status-of-the-art and prospect," *Shock and Vibration*, vol. 2021, Article ID 8767592, 15 pages, 2021.

[11] A. W. Khair, "An analysis of coal bump liability in a bump prone mine," *International Journal of Mining Engineering*, vol. 3, no. 4, pp. 243–259, 1985.

[12] Q. X. Qi, Z. H. Ouyang, S. K. Zhao, H. Y. Li, X. L. Li, and N. B. Zhang, "Study on types of rock burst mine and prevention methods in China," *Coal Science and Technology*, vol. 42, no. 10, pp. 1–5, 2014.

[13] F. Q. Gong, J. F. Pan, and Q. Jiang, "The difference analysis of rock burst and coal burst and key mechanisms of deep engineering geological hazards," *Journal of Engineering Geology*, vol. 29, no. 4, pp. 933–961, 2021.

[14] Q. X. Qi, Y. Z. Li, S. K. Zhao et al., "Seventy years development of coal mine rockburst in China: establishment and consideration of theory and technology system," *Coal Science and Technology*, vol. 47, no. 9 1, 40 pages, 2019.

[15] Q. X. Qi, S. B. Chen, H. X. Wang, D. B. Mao, and Y. X. Wang, "Study on the relations among rock burst, rockburst and mining tremor with numerical simulation," *Chinese Journal of Rock Mechanics and Engineering*, vol. 22, no. 11, pp. 1852–1858, 2003.

[16] Y. S. Pan, Z. H. Li, and M. T. Zhang, "Distribution, type, mechanism and prevention of rockburst in China," *Chinese Journal of Rock Mechanics and Engineering*, vol. 22, no. 11, pp. 1844–1851, 2003.

[17] Q. H. Qian, "Definition, mechanism, classification and quantitative forecast model for rockburst and pressure bump," *Rock and Soil Mechanics*, vol. 35, no. 1, pp. 1–6, 2014.

[18] C. Newman and D. Newman, "Numerical analysis for the prediction of bump prone conditions: a southern Appalachian pillar coal bump case study," *International Journal of Mining Science and Technology*, vol. 31, no. 1, pp. 75–81, 2021.

[19] K. Y. Zhou, L. M. Dou, X. W. Li et al., "Coal burst and mining-induced stress evolution in a deep isolated main entry area–A case study," *Engineering Failure Analysis*, vol. 137, Article ID 106289, 2022.

[20] H. Lawson, A. Weakley, and A. Miller, "Dynamic failure in coal seams: implications of coal composition for bump susceptibility," *International Journal of Mining Science and Technology*, vol. 26, no. 1, pp. 3–8, 2016.

[21] M. Javadi, G. Saeedi, and K. Shahriar, "Evaluation of coal bump risk during underground mining: a case study of tabas coal mine," *Journal of Failure Analysis and Prevention*, vol. 18, no. 6, pp. 1503–1515, 2018.

[22] Y. Z. Zhang, H. G. Ji, and Z. F. Hou, "Instability criterion of rockburst risk based on Mohr-Coulomb strength theory," *Metal Mine*, vol. 32, no. 11, pp. 138–142, 2014.

[23] J. P. Zuo, Y. Chen, and F. Cui, "Investigation on mechanical properties and rock burst tendency of different coal-rock combined bodies," *Journal of China University of Mining and Technology*, vol. 47, no. 1, pp. 81–87, 2018.

[24] Z. G. Deng, "Multi-field coupling dynamic evaluation method of rockburst hazard considering dynamic and static load," *Coal Science and Technology*, vol. 49, no. 4, pp. 121–132, 2021.

[25] M. T. Gao, Z. Q. Song, H. Q. Duan, H. Q. Xin, and J. Q. Tang, "Mechanical properties and control rockburst mechanism of coal and rock mass with bursting liability in deep mining," *Shock and Vibration*, vol. 2020, Article ID 8833863, 15 pages, 2020.

[26] D. Xu, M. S. Gao, Y. L. He, and X. Yu, "A study on the mechanical properties and bursting liability of coal-rock composites with seam partings," *Advances in Civil Engineering*, vol. 2021, Article ID 9953241, 13 pages, 2021.

[27] D. L. Ji, H. Cheng, H. B. Zhao, and C. Zhang, "Creep damage evolution and instability induction mechanism of the rock under impact disturbance," *Journal of China Coal Society*, 2023.

[28] Q. X. Qi, Y. Z. Li, H. T. Li et al., "Preliminary theoretical study on stress flow thought for rock burst and its control," *Journal of Mining and Safety Engineering*, vol. 38, no. 5, pp. 866–875, 2021.

[29] H. P. Xie, H. W. Zhou, D. J. Xue, H. W. Wang, R. Zhang, and F. Gao, "Research and consideration on deep coal mining and critical mining depth," *Journal of China Coal Society*, vol. 37, no. 4, pp. 535–542, 2012.

[30] H. P. Xie, F. Gao, Y. Ju et al., "Quantitative definition and investigation of deep mining," *Journal of China Coal Society*, vol. 40, no. 1, pp. 1–10, 2015.